Received: 28 June 2023 | Revised: 12 July 2023 | Accepted: 23 August 2023

DOI: 10.1002/pamm.202300058

RESEARCH ARTICLE

Efficient thermomechanically coupled FE-FFT-based multiscale simulation of polycrystals

Christian Gierden[1] | **Annika Schmidt**[1] | **Johanna Waimann**[1,2] | **Bob Svendsen**[3,4] | **Stefanie Reese**[1]

[1]Institute of Applied Mechanics, RWTH Aachen University, Aachen, Germany

[2]Modeling and Simulation Techniques for Systems of Polycrystalline Materials, RWTH Aachen University, Aachen, Germany

[3]Material Mechanics, RWTH Aachen University, Aachen, Germany

[4]Microstructure Physics and Alloy Design, Max-Planck-Institut für Eisenforschung GmbH, Düsseldorf, Germany

Correspondence
Christian Gierden, Institute of Applied Mechanics, RWTH Aachen University, Mies-van-der-Rohe-Straße 1, D-52074 Aachen, Germany.
Email: christian.gierden@ifam.rwth-aachen.de

Funding information
German Research Foundation, Grant/Award Numbers: 223500200, 417002380, 453596084, 454873500

Abstract

In general, the overall macroscopic material behavior of any structural component is directly dependent on its underlying microstructure. For metal components, the associated microstructure is given in terms of a polycrystal. To enable the simulation of the related microstructural and overall elasto-viscoplastic material behavior, a two-scale simulation approach can be used. In this context, we use a FE-FFT-based two-scale method, which is an efficient alternative to the classical FE^2 method for the simulation of periodic microstructures. In addition, we consider a thermomechanically coupled framework to account for both thermal and mechanical loads. Finally, we incorporate a model order reduction technique based on a coarsely discretized microstructure to develop an efficient two-scale simulation technique. As a demonstration of the feasibility of the proposed simulation framework, a numerical example will be investigated.

1 | INTRODUCTION

When studying the overall material behavior of a structural component, this behavior is directly determined by the underlying microstructure and its properties. For example, when analyzing metals, the microscale is represented by a polycrystal and its characteristics. In order to investigate both the macroscopic as well as the microscopic material behavior in a high resolution manner, several multiscale approaches have been developed [1]. The most common in this context is the application of the FE^2 method, which refers to the use of the finite element method on both scales [2, 3]. An alternative to this two-scale method is the FE-FFT-based method introduced in [4]. In this approach, the finite element simulation on the microscale is replaced by a Fast Fourier Transform (FFT)-based approach [5, 6]. This two-scale simulation method has been applied to the multiscale simulation of polycrystalline microstructures at small strains in [7] and generalized to finite strains in [8, 9]. Furthermore, an extension considering additionally a thermomechanical coupling with a constant

temperature field on the microscale at finite strains was introduced in [10]. A general review on FE-FFT-based two-scale methods is given in [11].

Considering only the microscale simulation, the FFT-based method was first applied to the simulation of polycrystalline microstructures considering rigid-viscoplastic material behavior at small strains in [12] and was found to be an efficient solution method for the simulation of periodic microstructures compared to the finite element method [13, 14]. A generalization of this approach to elasto-viscoplastic material behavior at small strains and further to finite strains can be found in [15] and [16], respectively. To increase the accuracy and efficiency of an FFT-based microscale simulation, several methods have been introduced. To mention some of them, finite difference approximations can be used to reduce the effect of Gibbs oscillations [17, 18] or efficient solvers such as conjugate gradient based solvers are applied to reduce the computational effort either in a small strain setting [19, 20] or in a finite strain setting [21]. A comprehensive review of the FFT-based microscale simulation technique can be found in [22, 23].

Since two-scale simulation methods are generally computationally demanding, several efficient solution strategies and model order reduction techniques have been developed to reduce this computational burden. Efficient solution strategies include methods based on a coarsely discretized microstructure for the two-scale simulation, while high-resolution results can be generated in a postprocessing step [24, 25], or methods using a pre-calculated database in general, while the high-resolution two-scale simulation is performed only in macroscopic critical areas [26]. Other model order reduction techniques reduce the computational effort at either the macro- or microscale. Since model order reduction techniques are widely used for macroscale simulations, only specific model order reduction techniques applied to FFT-based microscale simulations are addressed here. In this context, the computational costs of FFT-based microscale simulations have been reduced using proper orthogonal decomposition [27], low-rank tensor approximations [28], or a reduced set of Fourier modes [29] with a fixed [29], geometrically adapted [30], or strain-based [31] sampling pattern, or additionally combined with a clustered microstructure [32].

In this work, we use the thermomechanically coupled FE-FFT-based two-scale method incorporating finite strains introduced in [10] to compute fluctuating temperature fields at the microscale, similar to what was done in [33, 34], using a FE-based microstructure simulation. Here, the FFT-based microscale simulation is utilized and optimized using the finite difference approximation presented in [18] and a Newton–Krylov solver as introduced in [21]. In addition, the efficient solution strategy based on a coarsely discretized microstructure for the two-scale simulation [24, 25] is applied.

The paper is organized as follows: in Section 2, the thermomechanically coupled two-scale boundary value problem is briefly discussed. This is followed by the introduction of the microstructural constitutive relations in Section 3. After discussing the microscale simulation using spectral solvers in Section 4 and the numerical results in Section 5, the paper ends with a conclusion and an outlook in Section 6.

2 | TWO-SCALE BOUNDARY VALUE PROBLEM

To perform a thermomechanically coupled two-scale simulation, the balance of linear momentum and the balance of internal energy must be solved at the macroscale as well as the microscale. Considering finite strains, these balance equations with respect to the reference configuration are given below, while a sketch of the two-scale boundary value problem considering deformed bodies is given on the left:

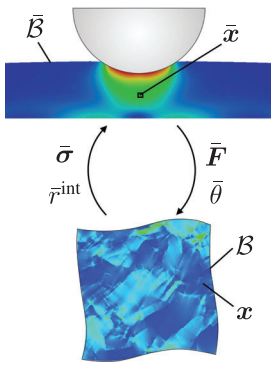

Balance of linear momentum

Macroscale

$$\begin{aligned} \text{Div}\left(\bar{\boldsymbol{F}}\bar{\boldsymbol{S}}\right) + \bar{\boldsymbol{f}}_0 &= \boldsymbol{0} && \text{in } \bar{\mathcal{B}}_0 \\ \bar{\boldsymbol{F}}\bar{\boldsymbol{S}}\cdot\bar{\boldsymbol{N}} &= \bar{\boldsymbol{t}}_0 && \text{on } \partial_{\boldsymbol{t}}\bar{\mathcal{B}}_0 \\ \bar{\boldsymbol{u}} &= \bar{\boldsymbol{u}}_0 && \text{on } \partial_{\boldsymbol{u}}\bar{\mathcal{B}}_0 \end{aligned}$$

Microscale

$$\begin{aligned} &\text{Div}\left(\boldsymbol{F}\boldsymbol{S}\right) = \boldsymbol{0} \quad \text{in } \mathcal{B}_0 \\ &\boldsymbol{S} = \boldsymbol{S}(\bar{\boldsymbol{X}}, \boldsymbol{X}, \boldsymbol{F}(\bar{\boldsymbol{X}}, \boldsymbol{X}), \theta(\bar{\boldsymbol{X}}), \zeta_k(\bar{\boldsymbol{X}}, \boldsymbol{X})) \\ &\boldsymbol{F} = \bar{\boldsymbol{F}}\left(\bar{\boldsymbol{X}}\right) + \tilde{\boldsymbol{H}}\left(\bar{\boldsymbol{X}}, \boldsymbol{X}\right) \end{aligned}$$

Balance of internal energy

Macroscale

$$\begin{aligned} -\dot{\bar{e}} + \bar{\boldsymbol{S}} : \dot{\bar{\boldsymbol{E}}} - \text{Div}\left(\bar{\boldsymbol{q}}_0\right) + \bar{r}_0^{\text{ext}} &= 0 && \text{in } \bar{\mathcal{B}}_0 \\ \bar{\boldsymbol{q}}_0 \cdot \bar{\boldsymbol{N}} &= -\bar{q}_0 && \text{on } \partial_{\boldsymbol{q}}\bar{\mathcal{B}}_0 \\ \bar{\theta} &= \bar{\theta}_0 && \text{on } \partial_{\theta}\bar{\mathcal{B}}_0 \end{aligned}$$

Microscale

$$\begin{aligned} &-\dot{e} + \boldsymbol{S} : \dot{\boldsymbol{E}} - \text{Div}\left(\boldsymbol{q}_0\right) = 0 \quad \text{in } \mathcal{B}_0 \\ &r_0^{\text{int}} = r_0^{\text{int}}(\bar{\boldsymbol{X}}, \boldsymbol{X}, \boldsymbol{F}(\bar{\boldsymbol{X}}, \boldsymbol{X}), \theta(\bar{\boldsymbol{X}}), \zeta_k(\bar{\boldsymbol{X}}, \boldsymbol{X})) \\ &\theta \quad = \bar{\theta}\left(\bar{\boldsymbol{X}}\right) + \tilde{\theta}\left(\bar{\boldsymbol{X}}, \boldsymbol{X}\right) \end{aligned}$$

Here $\boldsymbol{X}$ represents the position vector, $\boldsymbol{F}$ is the deformation gradient, $\boldsymbol{E}$ is the Green–Lagrange strain, $\boldsymbol{S}$ is the second Piola–Kirchhoff stress, $\boldsymbol{f}_0$ is an external body force, $\boldsymbol{t}_0$ is a surface traction, e is the total energy, $\boldsymbol{q}_0$ is the heat flux, r_0^{ext} and r_0^{int} define the external and internal heat sources, and ζ_k represents a set of internal variables. The bar above any quantity refers to the macroscale, and the absence of the bar therefore refers to the microscale. Furthermore the macroscopic balance equations must be fulfilled within the body $\bar{\mathcal{B}}_0$ and satisfy the macroscopic boundary conditions as given on $\partial\bar{\mathcal{B}}_0$, while the microscopic balance equations must be fulfilled within the unit cell $\mathcal{B}_0$ assuming periodic boundary conditions. Finally, $\tilde{\boldsymbol{H}}$ and $\tilde{\theta}$ are the microscopic fluctuating displacement gradient and temperature, which denote the primary unknowns.

As introduced in [33], the microscopic boundary value problem is solved in a staggered manner. First, the balance of linear momentum is solved by applying $\bar{\boldsymbol{F}}$ and considering the temperature field $\theta = \bar{\theta}$ to be constant, to compute the averaged stress $\bar{\boldsymbol{S}}$ and internal heat sources $\bar{r}_0^{\text{int}}$ (which are involved in the macroscopic balance of internal energy; cf. Equation (6)). Then, the balance of internal energy is solved by employing the macroscopic temperature gradient $\text{Grad}(\bar{\theta})$ to compute the averaged heat flux $\bar{\boldsymbol{q}}_0$. However, since we only consider an isotropic and homogeneous conductivity K_θ within the microstructure, the microstructural fluctuations can be neglected. Thus, in contrast to [33], the macroscopic heat flux $\bar{\boldsymbol{q}}_0$ can be computed directly from the macroscopic quantities without solving the microscopic balance of internal energy. Therefore, the scale transition back to the macroscale is performed by calculating only the macroscopic second Piola–Kirchhoff stress $\bar{\boldsymbol{S}}$ and the macroscopic heat sources $\bar{r}_0^{\text{int}}$ as volume averages of their microscopic counterparts, where $\mathcal{V}_0$ is the volume of the microstructure:

$$\bar{\boldsymbol{S}}(\bar{\boldsymbol{X}}) = \frac{1}{\mathcal{V}_0}\int_{\mathcal{B}_0} \boldsymbol{S}(\bar{\boldsymbol{X}},\boldsymbol{X})\,\mathrm{d}\mathcal{V} \quad \text{and} \quad \bar{r}_0^{\text{int}}(\bar{\boldsymbol{X}}) = \frac{1}{\mathcal{V}_0}\int_{\mathcal{B}_0} r_0^{\text{int}}(\bar{\boldsymbol{X}},\boldsymbol{X})\,\mathrm{d}\mathcal{V}\,.$$

3 | MICROSTRUCTURAL CONSTITUTIVE MODEL

Considering a two-scale simulation of metals, the associated microstructure is defined as a polycrystal. Taking into account finite deformations, the deformation gradient $\boldsymbol{F} = \boldsymbol{F}_e\boldsymbol{F}_p$ is multiplicatively split into an elastic part $\boldsymbol{F}_e$ and a plastic part $\boldsymbol{F}_p$. Furthermore, in the context of crystal plasticity, where dislocation slip is assumed to be the only plastic deformation process, the plastic velocity gradient $\boldsymbol{L}_p = \dot{\boldsymbol{F}}_p\boldsymbol{F}_p^{-1}$ is given as the sum of each shear rate $\dot{\gamma}_\alpha$ over all slip systems n_α defined by the slip plane normal $\boldsymbol{n}_\alpha$ and the slip plane direction $\boldsymbol{d}_\alpha$ [35, 36]:

$$\boldsymbol{L}_p = \sum_{\alpha}^{n_\alpha} \dot{\gamma}_\alpha\, \boldsymbol{d}_\alpha \otimes \boldsymbol{n}_\alpha\,. \tag{1}$$

Since elastic deformations in metals are generally small, we applied a St. Venant–Kirchhoff law, taking into account the effect of temperature changes, which defines the elastic second Piola–Kirchhoff stress in the intermediate configuration as

$$\boldsymbol{S}_e = \mathbb{C}^{\text{gra}} : \boldsymbol{E}_e - \mathbb{C}^{\text{gra}} : \boldsymbol{A}_t\,(\theta - \theta^{\text{ref}})\,. \tag{2}$$

In the previous equation, the rotated cubic anisotropic elasticity tensor $\mathbb{C}^{\text{gra}}$ depending on the grain orientation, the elastic Green–Lagrange strain $\boldsymbol{E}_e$, the reference temperature θ^{ref}, and the thermal expansion tensor $\boldsymbol{A}_t = \alpha_t\boldsymbol{I}$ were introduced with α_t denoting the thermal expansion coefficient and $\boldsymbol{I}$ referring to the second-order identity tensor. Furthermore, we considered an isotropic hardening $q_p(\gamma_{\text{acc}})$ of Voce-type plus an additional linear term depending on the accumulated plastic slip γ_{acc}, which is defined as the time integral over the sum of all shear rates. Finally, the evolution equation for the shear rate in each slip system is assumed to be of Perzyna-type yielding

$$\dot{\gamma}_\alpha = \begin{cases} 0 & \text{if}\, \tau_\alpha \le \tau^c \\ \operatorname{sgn}(\tau_\alpha)\,\dot{\gamma}_0 \left(\frac{|\tau_\alpha| - \tau^c}{\tau^D}\right)^p & \text{if}\, \tau_\alpha > \tau^c \end{cases}, \tag{3}$$

with the resolved shear stress $\tau_\alpha = \boldsymbol{M}_e : (\boldsymbol{d}_\alpha \otimes \boldsymbol{n}_\alpha)$ in slip system α, the critical shear stress τ^c, the drag stress τ^D, the rate sensitivity parameter p, and the reference shear rate $\dot{\gamma}_0$.

4 | MICROSCALE SIMULATION USING A SPECTRAL SOLVER

Since solving the macroscopic boundary value problem by means of the finite element method is a very common procedure, in the following we will focus only on solving the microscopic boundary value problem by means of a spectral solver. As mentioned before, the solutions of the mechanical and thermal boundary value problems are computed in a staggered manner. Starting from the mechanical boundary value problem and using the FFT-based simulation approach [5, 6], the microscopic balance equation has to be reformulated by introducing the polarization stress $\boldsymbol{\tau}$ [37], which defines the difference between the stress in the real microstructure and the stress in an isotropic homogeneous reference material defined by the stiffness tensor $\mathbb{C}^0$:

$$\begin{aligned} \operatorname{Div}\left(\boldsymbol{\tau} + \mathbb{C}^0 : \boldsymbol{F}\right) &= \boldsymbol{0} \quad \text{in} \mathcal{B}_0 \\ \boldsymbol{\tau} &= \boldsymbol{F}\boldsymbol{S} - \mathbb{C}^0 : \boldsymbol{F} \\ \boldsymbol{F} &= \bar{\boldsymbol{F}} + \tilde{\boldsymbol{H}} \end{aligned}$$

This reformulated boundary value can be solved using the Lippmann–Schwinger equation [38] yielding

$$\boldsymbol{F} = \bar{\boldsymbol{F}} - \boldsymbol{\Gamma}^0 * \boldsymbol{\tau}\,, \tag{4}$$

where $\boldsymbol{\Gamma}^0$ is the Green's operator and $*$ represents the convolution of the Green's operator and the polarization stress, which considers the influence of $\boldsymbol{\tau}$ on $\boldsymbol{F}$ at each position. Transferring this equation in Fourier space results in

$$\hat{\boldsymbol{F}}(\boldsymbol{\xi}) = \begin{cases} -\hat{\boldsymbol{\Gamma}}^0(\boldsymbol{\xi}) : \hat{\tau}(\boldsymbol{\xi}) & \text{for} \, \boldsymbol{\xi} \neq \boldsymbol{0} \\ \bar{\boldsymbol{F}} & \text{for} \, \boldsymbol{\xi} = \boldsymbol{0} \end{cases}. \tag{5}$$

Here, the hat over any quantity refers to its Fourier transform depending on the Fourier modes $\boldsymbol{\xi}$. In Fourier space, the convolution results in a simple multiplication and the Green's operator is explicitly known in Fourier space, depending only on the reference material behavior and the Fourier modes. In order to solve this equation, we use a Newton–Krylov solver as introduced in [21].

To compute microstructural fluctuations in the temperature field, the thermal boundary value problem is also solved in Fourier space. Therefore the balance of internal energy with respect to the reference configuration is reformulated as

$$-\theta \frac{\partial^2 \check{\psi}}{\partial \theta^2}\,\dot{\theta} = \underbrace{\theta \frac{\partial \boldsymbol{S}}{\partial \theta} : \dot{\boldsymbol{E}}}_{r_0^e} + \underbrace{\left[\sum_{\alpha=1}^{n} \dot{\gamma}_\alpha \left(\tau_\alpha - \theta \frac{\partial \tau_\alpha}{\partial \theta}\right)\right] - \left(q_p - \theta \frac{\partial q_p}{\partial \theta}\right)\dot{\gamma}_{\text{acc}}}_{r_0^p} - \operatorname{Div}(\boldsymbol{q}_0)\,. \tag{6}$$

with the total energy $\check{\psi}$. By considering a constant temperature field in time during the microscale simulation and by neglecting the elastic heat sources r_0^e, while simplifying the plastic heat sources r_0^p to

$$r_0^p \approx \beta \left(\sum_{\alpha=1}^{n} \dot{\gamma}_\alpha \, \tau_\alpha - q_p \, \dot{\gamma}_{\text{acc}} \right) \tag{7}$$

using the Taylor–Quinney coefficient β [39], the balance of internal energy in the current configuration reduces to

$$\operatorname{div}(\boldsymbol{q}) - r^p = 0 \tag{8}$$

with $r^p = 1/\det(\boldsymbol{F})\, r_0^p$. Considering $\boldsymbol{q} = -K_\theta \operatorname{grad}(\theta)$ and an isotropic and homogeneous conductivity K_θ for each crystal, this equation can directly be solved in Fourier space:

$$\hat{\theta}(\boldsymbol{\xi}) = \begin{cases} -\dfrac{\hat{r}^p(\boldsymbol{\xi})}{K_\theta \, \boldsymbol{\xi} \cdot \boldsymbol{\xi}} & \text{for} \, \boldsymbol{\xi} \neq \boldsymbol{0} \\ \bar{\theta} & \text{for} \, \boldsymbol{\xi} = \boldsymbol{0} \end{cases} \tag{9}$$

and later transferred back to real space.

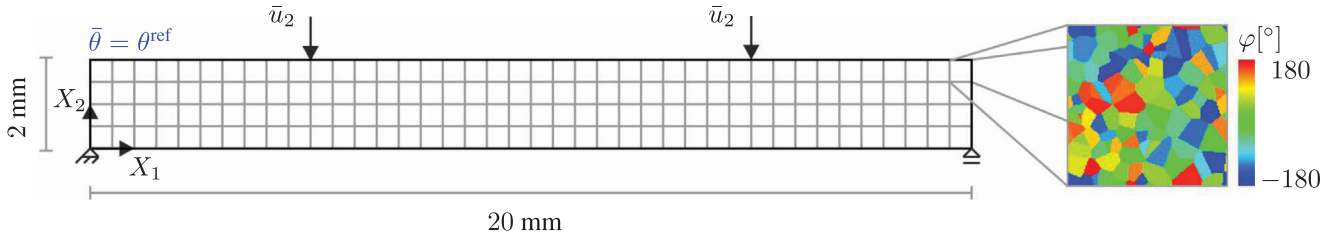

FIGURE 1 Macroscopic boundary value problem with dimensions, boundary conditions, and discretization of the four-point bending test and orientation of the first Euler angle of the polycrystalline microstructure.

5 | NUMERICAL RESULTS

To demonstrate the applicability of the thermomechanically coupled FE-FFT-based two-scale method, we investigate the multiscale simulation of a four-point bending test considering a polycrystalline microstructure and the material parameters of copper, chosen in line with the literature. The dimensions, boundary conditions, and discretization of the macroscopic boundary value problem are depicted in Figure 1. The polycrystalline microstructure with the orientation of the first Euler angle is shown on the right. A displacement of $u_2 = 0.5\,\text{mm}$ is applied within 1 s, and the simulation is performed at room temperature
$\theta^{\text{ref}} = 293.15\,\text{K}$.

The two-scale simulation is performed using Abaqus, with the FFT-based microstructure simulation implemented as a user material. On the macroscale, a fully coupled thermomechanical finite element analysis is performed. In this context, a plane strain setting and reduced integration with hourglass stabilization are considered.

Regarding the microscale simulation, we use an efficient solution strategy [24, 25] based on using only a coarsely discretized microstructure during the two-scale simulation, which is attached to each macroscopic integration point. Since this only provides accurate macroscopic results, highly resolved microstructural results are generated in a postprocessing step by applying the macroscopic deformation gradient of any integration point of particular interest to a finely discretized microstructure.

The results of the two-scale simulation are given in Figure 2. At the macroscale, the logarithmic strain $\overline{LE}_{11}$, the Cauchy stress $\bar{\sigma}_{11}$, the accumulated plastic slip $\bar{\gamma}_{\text{acc}}$, and the change in the temperature $\Delta\bar{\theta} = \bar{\theta} - \theta^{\text{ref}}$ are shown, whereas at the microscale, the Green–Lagrange strain E_{11}, the Cauchy stress σ_{11}, the accumulated plastic slip γ_{acc}, and the fluctuating temperature field $\tilde{\theta}$ are plotted. The microsopic results are generated for the highlighted element at the macroscale.

As expected, the maximum values within the macroscopic fields are located between the two loads and are more or less constant in the four-point bending test. Looking at the strain in horizontal direction, the compressive strains are located at the top of the specimen, while the tensile strains occur at the bottom of the specimen. This behavior is similar for the stress. Considering the accumulated plastic slip, it can be seen that a higher amount of plastic deformation occurs in the tensile regime. Since the temperature change in our model only depends on the evolution of the plastic deformations, the maximum temperature change in the specimen is directly related to the presence of the accumulated plastic slip. The microscopic results reveal that due to grain boundaries there are local peaks with values significantly higher than the average for strain, stress and accumulated plastic slip. Additionally, the correlation between plastic deformations and the temperature evolution is again clearly visible. Since the changes within the temperature field are rather small, only the fluctuating temperature field $\tilde{\theta} = \theta - \bar{\theta}$ is plotted. Hence, the field fluctuates around zero. This explains the negative values, which are not related to a cooling.

6 | CONCLUSION AND OUTLOOK

In this work, we presented a thermomechanically coupled FE-FFT-based two-scale model for the simulation of polycrystalline microstructures. We considered not only fluctuating mechanical fields such as the strain, but also fluctuating thermal fields. The applicability of the model is demonstrated by considering the two-scale simulation of a four-point bending test of a copper specimen. It shows that due to plastic deformation, heat is generated in the specimen, which fluctuates as desired on the microscale.

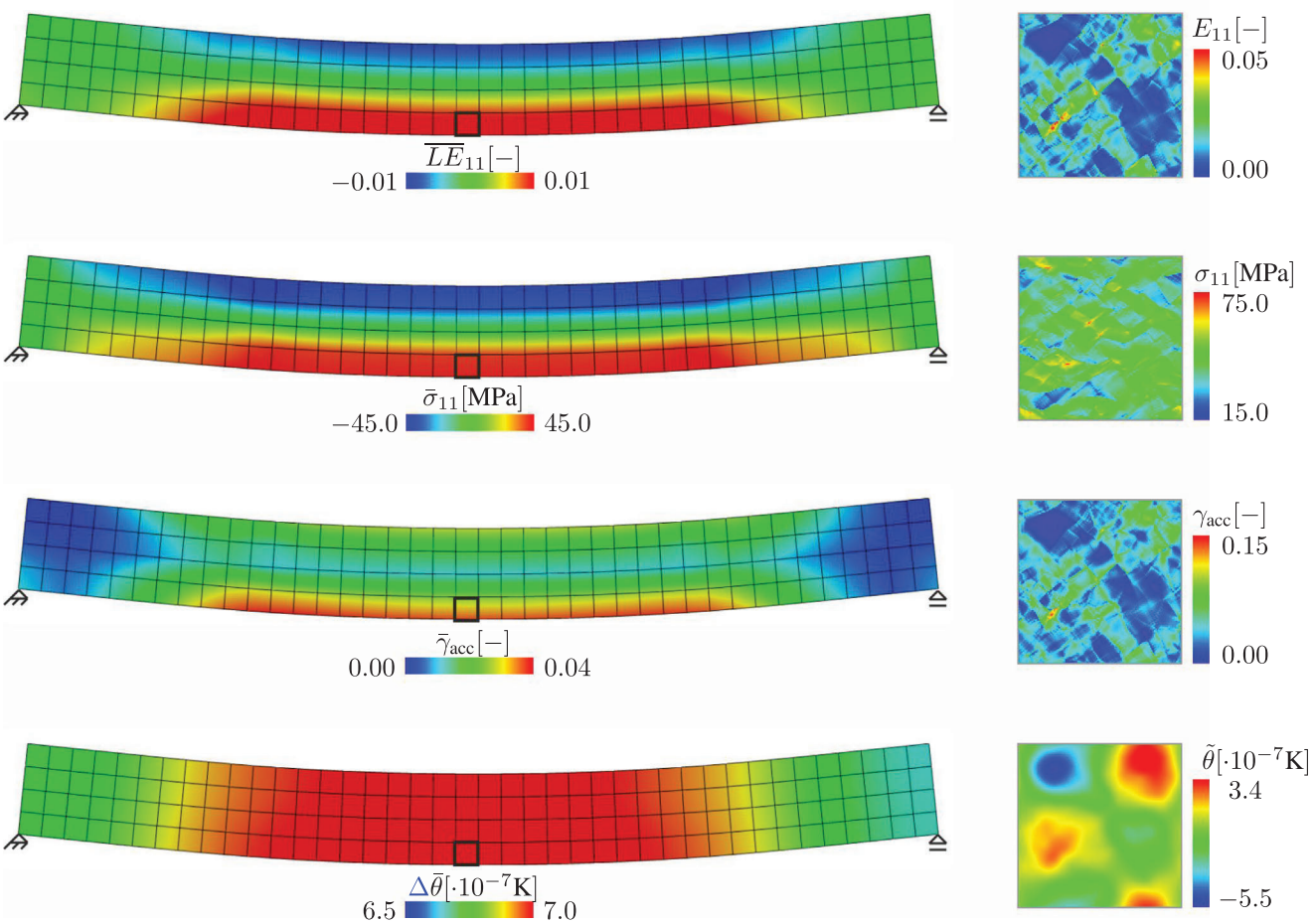

FIGURE 2 Macroscopic and microscopic results for the marked element of the strain, Cauchy stress, accumulated plastic slip as well as the change in the macroscopic temperature and microscopically fluctuating temperature field are shown for the maximum applied displacement.

However, the evolution of heat on the macroscale as well as the local fluctuations of the temperature on the microscale are rather small. Therefore, future work will deal with the investigation of different materials, such as shape memory alloys. In this context, microscopic phenomena such as martensitic phase transformations occur and will be modeled (e.g., shown for mechanically induced phase transformations in [40]). These martensitic phase transformations lead to an additional heat generation and therefore the temperature evolution is expected to be much higher. Vice versa, phase transformations induced by the temperature will also occur in this context (see e.g. [41]) and have to be captured.

ACKNOWLEDGMENTS

The authors gratefully acknowledge the financial support of the research work by the German Research Foundation (DFG, Deutsche Forschungsgemeinschaft) within the transregional Collaborative Research Center SFB/TRR 136, project number 223500200, subprojects M03 and M05 for the years 2014–2022. In addition, Stefanie Reese gratefully acknowledges the financial support of the research work by the German Research Foundation (DFG, Deutsche Forschungsgemeinschaft) within the transregional Collaborative Research Center SFB/TRR 280, project number 417002380, subproject A01 as well as the transregional Collaborative Research Center SFB/TRR 339, project number 453596084, subproject B05 and the project RE 1057/52-1, project number 454873500.

Open access funding enabled and organized by Projekt DEAL.

ORCID

Christian Gierden https://orcid.org/0000-0003-1978-3570
Annika Schmidt https://orcid.org/0000-0003-1422-9263
Johanna Waimann https://orcid.org/0000-0002-7579-7240

REFERENCES

1. Geers, M. G. D., Kouznetsova, V. G., & Brekelmans, W. A. M. (2010). Multi-scale computational homogenization: Trends and challenges. *Journal of Computational and Applied Mathematics*, *234*(7), 2175–2182.
2. Smit, R. J. M., Brekelmans, W. A. M., & Meijer, H. E. H. (1998). Prediction of the mechanical behavior of nonlinear heterogeneous systems by multi-level finite element modeling. *Computer Methods in Applied Mechanics and Engineering*, *155*(1-2), 181–192.
3. Feyel, F., & Chaboche, J.-L. (2000). FE^2 multiscale approach for modelling the elasto-viscoplastic behaviour of long fibre SiC/Ti composite materials. *Computer Methods in Applied Mechanics and Engineering*, *183*(3-4), 309–330.
4. Spahn, J., Andrä, H., Kabel, M., & Müller, R. (2014). A multiscale approach for modeling progressive damage of composite materials using fast Fourier transforms. *Computer Methods in Applied Mechanics and Engineering*, *268*, 871–883.
5. Moulinec, H., & Suquet, P. (1994). A fast numerical method for computing the linear and nonlinear mechanical properties of composites, Comptes rendus de l'Académie des sciences. *Série II, Mécanique, Physique, Chimie, Astronomie*, *318*, 1417–1423.
6. Moulinec, H., & Suquet, P. (1998). A numerical method for computing the overall response of nonlinear composites with complex microstructure. *Computer Methods in Applied Mechanics and Engineering*, *157*(1-2), 69–94.
7. Kochmann, J., Wulfinghoff, S., Reese, S., Mianroodi, J. R., & Svendsen, B. (2016). Two-scale FE-FFT- and phase-field-based computational modeling of bulk microstructural evolution and macroscopic material behavior. *Computer Methods in Applied Mechanics and Engineering*, *305*, 89–110.
8. Kochmann, J., Brepols, T., Wulfinghoff, S., Svendsen, B., & Reese, S. (2018). On the computation of the exact overall consistent tangent moduli for non-linear finite strain homogenization problems using six finite perturbations. *6th European Conference on Computational Mechanics (ECCM 6)*.
9. Han, F., Roters, F., & Raabe, D. (2020). Microstructure-based multiscale modeling of large strain plastic deformation by coupling a full-field crystal plasticity-spectral solver with an implicit finite element solver. *International Journal of Plasticity*, *125*, 97–117.
10. Schmidt, A., Gierden, C., Waimann, J., Svendsen, B., & Reese, S. (2023). Two-scale FE-FFT-based thermomechanically coupled modeling of elasto-viscoplastic polycrystalline materials at finite strains. *Proceedings in Applied Mathematics and Mechanics*, *22*(1), e202200172.
11. Gierden, C., Kochmann, J., Waimann, J., Svendsen, B., & Reese, S. (2022). A review of FE-FFT-based two-scale methods for computational modeling of microstructure evolution and macroscopic material behavior. *Archives of Computational Methods in Engineering*, *29*, 4115–4135.
12. Lebensohn, R. A. (2001). N-site modeling of a 3D viscoplastic polycrystal using Fast Fourier Transform. *Acta Materialia*, *49*(14), 2723–2737.
13. Prakash, A., & Lebensohn, R. A. (2009). Simulation of micromechanical behavior of polycrystals: Finite elements versus fast Fourier transforms. *Modelling and Simulation in Materials Science and Engineering*, *17*(6), 064010.
14. Liu, B., Raabe, D., Roters, F., Eisenlohr, P., & Lebensohn, R. A. (2010). Modelling and simulation in materials science and engineering comparison of finite element and fast Fourier transform crystal plasticity solvers for texture prediction. *Modelling and Simulation in Materials Science and Engineering*, *18*(8), 085005.
15. Lebensohn, R. A., Kanjarla, A. K., & Eisenlohr, P. (2012). An elasto-viscoplastic formulation based on fast Fourier transforms for the prediction of micromechanical fields in polycrystalline materials. *International Journal of Plasticity*, *32*, 59–69.
16. Eisenlohr, P., Diehl, M., Lebensohn, R. A., & Roters, F. (2013). A spectral method solution to crystal elasto-viscoplasticity at finite strains. *International Journal of Plasticity*, *46*, 37–53.
17. Müller, W. H. (1998). Fourier transforms and their application to the formation of textures and changes of morphology in solids. *Solid Mechanics and Its Applications*, *60*, 61–72.
18. Willot, F. (2015). Fourier-based schemes for computing the mechanical response of composites with accurate local fields. *Comptes Rendus Mécanique*, *343*(3), 232–245.
19. Zeman, J., Vodřejc, J., Novák, J., & Marek, I. (2010). Accelerating a FFT-based solver for numerical homogenization of periodic media by conjugate gradients. *Journal of Computational Physics*, *229*(21), 8065–8071.
20. Gélébart, L., & Mondon-Cancel, R. (2013). Non-linear extension of FFT-based methods accelerated by conjugate gradients to evaluate the mechanical behavior of composite materials. *Computational Materials Science*, *77*, 430–439.
21. Kabel, M., Böhlke, T., & Schneider, M. (2014). Efficient fixed point and Newton-Krylov solvers for FFT-based homogenization of elasticity at large deformations. *Computational Mechanics*, *54*, 1497–1514.
22. Schneider, M. (2021). A review of nonlinear FFT-based computational homogenization methods. *Acta Mechanica*, *232*, 2051–2100.
23. Lucarini, S., Upadhyay, M. V., & Segurado, J. (2021). FFT based approaches in micromechanics: Fundamentals, methods and applications. *Modelling and Simulation in Materials Science and Engineering*, *30*, 023002.
24. Kochmann, J., Wulfinghoff, S., Ehle, L., Mayer, J., Svendsen, B., & Reese, S. (2018). Efficient and accurate two-scale FE-FFT-based prediction of the effective material behavior of elasto-viscoplastic polycrystals. *Computational Mechanics*, *61*, 751–764.
25. Gierden, C., Kochmann, J., Waimann, J., Kinner-Becker, T., Sölter, J., Svendsen, B., & Reese, S. (2021). Efficient two-scale FE-FFT-based mechanical process simulation of elasto-viscoplastic polycrystals at finite strains. *Computer Methods in Applied Mechanics and Engineering*, *374*, 113566.
26. Köbler, J., Magino, N., Andrä, H., Welschinger, F., Müller, R., & Schneider, M. (2021). A computational multi-scale model for the stiffness degradation of short-fiber reinforced plastics subjected to fatigue loading. *Computer Methods in Applied Mechanics and Engineering*, *373*, 113522.
27. Garcia-Cardona, C., Lebensohn, R., & Anghel, M. (2017). Parameter estimation in a thermoelastic composite problem via adjoint formulation and model reduction. *International Journal for Numerical Methods in Engineering*, *112*(6), 578–600.

28. Vondřejc, J., Liu, D., Ladecký, M., & Matthies, H. G. (2020). FFT-based homogenisation accelerated by low-rank tensor approximations. *Computer Methods in Applied Mechanics and Engineering*, *364*, 112890.
29. Kochmann, J., Manjunatha, K., Gierden, C., Wulfinghoff, S., Svendsen, B., & Reese, S. (2019). A simple and flexible model order reduction method for FFT-based homogenization problems using a sparse sampling technique. *Computer Methods in Applied Mechanics and Engineering*, *347*, 622–638.
30. Gierden, C., Waimann, J., Svendsen, B., & Reese, S. (2021). A geometrically adapted reduced set of frequencies for a FFT-based microstructure simulation. *Computer Methods in Applied Mechanics and Engineering*, *386*, 114131.
31. Gierden, C., Waimann, J., Svendsen, B., & Reese, S. (2021). FFT-based simulation using a reduced set of frequencies adapted to the underlying microstructure. *Computer Methods in Materials Science*, *21*(1), 51–58.
32. Waimann, J., Gierden, C., Schmidt, A., Svendsen, B., & Reese, S. (2022). Reduced FFT-based simulation of a mechanically loaded clustered microstructure using an adaptive set of Fourier modes. *Key Engineering Materials*, *926*, 2285–2292.
33. Temizer, I., & Wriggers, P. (2011). Homogenization in finite thermoelasticity. *Journal of the Mechanics and Physics of Solids*, *59*(2), 344–372.
34. Li, J., Romero, I., & Segurado, J. (2019). Development of a thermomechanically coupled crystal plasticity modeling framework: Application to polycrystalline homogenization. *International Journal of Plasticity*, *119*, 313–330.
35. Rice, J. R. (1971). Inelastic constitutive relations for solids: An internal-variable theory and its application to metal plasticity. *Journal of the Mechanics and Physics of Solids*, *19*(6), 433–455.
36. Asaro, R. J., & Rice, J. R. (1977). Strain localization in ductile single crystals. *Journal of the Mechanics and Physics of Solids*, *25*(5), 309–338.
37. Hashin, Z., & Shtrikman, S. (1962). On some variational principles in anisotropic and nonhomogeneous elasticity. *Journal of the Mechanics and Physics of Solids*, *10*(4), 335–342.
38. Kröner, E. (1959). Allgemeine Kontinuumstheorie der Versetzungen und Eigenspannungen. *Archive for Rational Mechanics and Analysis*, *4*, 273–334.
39. Taylor, G. I., & Quinney, H. (1934). The latent energy remaining in a metal after cold working. *Proceedings of the Royal Society of London*, *143*(849), 307–326.
40. Waimann, J., Gierden, C., & Reese, S. (2022). Simulation of phase transformations in polycrystalline shape memory alloys using fast Fourier transforms. *ECCOMAS Congress 2022-8th European Congress on Computational Methods in Applied Sciences and Engineering*.
41. Waimann, J., & Reese, S. (2022). Variational modeling of temperature induced and cooling-rate dependent phase transformations in polycrystalline steel. *Mechanics of Materials*, *170*, 104299.

How to cite this article: Gierden, C., Schmidt, A., Waimann, J., Svendsen, B., & Reese, S. (2023). Efficient thermomechanically coupled FE-FFT-based multiscale simulation of polycrystals. *Proceedings in Applied Mathematics and Mechanics*, *23,* e202300058. https://doi.org/10.1002/pamm.202300058